SINTEF
PROCEEDINGS 5

International Conference Organised by IBPSA-Nordic, 13th–14th October 2020, OsloMet

BuildSIM-Nordic 2020

Selected papers

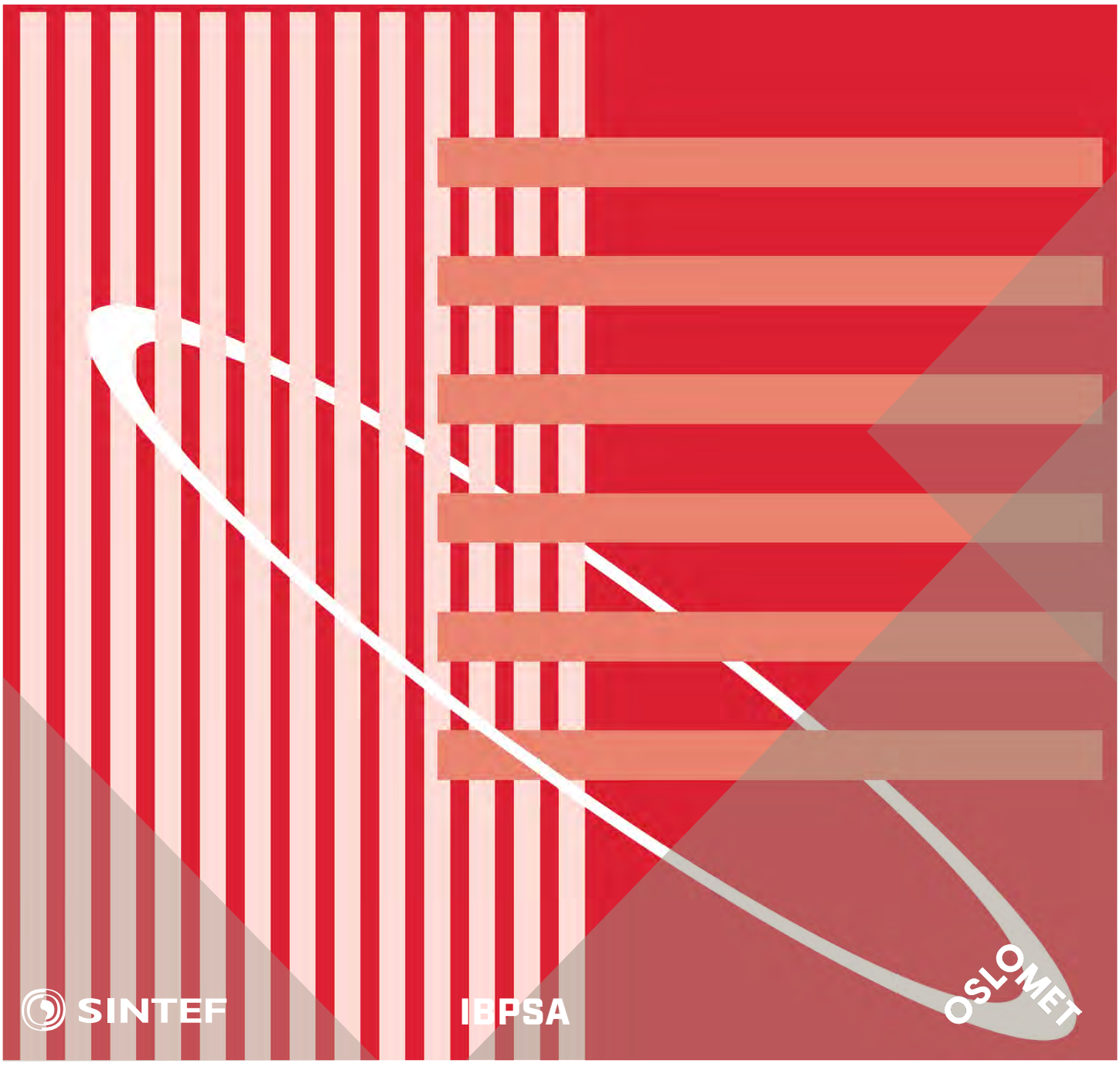

SINTEF Proceedings

Editors:
Laurent Georges, Matthias Haase, Vojislav Novakovic and Peter G. Schild

BuildSIM-Nordic 2020

Selected papers

International Conference Organised by IBPSA-Nordic,
13th–14th October 2020, OsloMet

SINTEF Academic Press

SINTEF Proceedings no 5
Editors:
Laurent Georges, Matthias Haase, Vojislav Novakovic and Peter G. Schild
BuildSIM-Nordic 2020
Selected papers
International Conference Organised by IBPSA-Nordic,
13th–14th October 2020, OsloMet

Keywords:
Building acoustics, Building Information Modelling (BIM), Building physics, CFD and air flow, Commissioning and control, Daylighting and lighting, Developments in simulation, Education in building performance simulation, Energy storage, Heating, Ventilation and Air Conditioning (HVAC), Human behavior in simulation, Indoor Environmental Quality (IEQ), New software developments, Optimization, Simulation at urban scale, Simulation to support regulations, Simulation vs reality, Solar energy systems, Validation, calibration and uncertainty, Weather data & Climate adaptation, Fenestration (windows & shading), Zero Energy Buildings (ZEB), Emissions and Life Cycle Analysis

Cover illustration: IBPSA-logo

ISSN 2387-4295 (online)
ISBN 978-82-536-1679-7 (pdf)

SINTEF Academic Press
Address: Børrestuveien 3
PO Box 124 Blindern
N-0314 OSLO
Tel: +47 40 00 51 00

www.sintef.no/community
www.sintefbok.no

Identifying grey-box models of Norwegian apartment block archetypes

Marius Bagle[1*], Harald Taxt Walnum[1], Igor Sartori[1]
[1]SINTEF Community, Oslo, Norway

** corresponding author: marius.bagle@sintef.no*

Abstract

Identification of grey-box models to describe the heat dynamics of buildings is treated extensively in literature, However, to identify these models, data from controlled heating experiments is needed, which is not feasible in many cases. In this work, the aim is to overcome this threshold by using datasets from simulations of detailed white-box models to identify the grey-box models. Given that the white-box models are validated and calibrated against real measurement data, the need for real measurement data is bypassed, thus enabling the use of grey-box models identified from simulation data in real - world predictive controllers. The results show that a three-state grey-box model is able to capture the heat dynamics of the white-box model over a time period of ~1 week in the summer months.

Introduction

A potentially large amount of flexibility resides in the space heating of residential buildings. To realize this potential, it is necessary to model heat demand with models that are accurate enough and suitable for real time control. Purely physical (white-box) models are ill-suited for the purpose due to the level of detail required, the high uncertainties associated with knowledge of key technical parameters and the difficulty to treat non-technical features such as user behavior. Well-suited for this purpose are grey-box models, which combine a relatively simple physical descriptions of the building with data-driven inference of key parameters. In (Xingji Y., Laurent, & Sartori, 2019), the validation performance of grey-box models based on physical knowledge of buildings and grey-box models extracted from technical standards are compared. In (Walnum, Sartori, & Lindberg, 2019), a backward selection procedure is used; by removing elements in the model and testing the different permutations in validation. In both papers, measurement data from a controlled heating experiment on a real building is used. This is the challenge with grey-box models. In addition to energy use and weather data, the indoor temperature should also be known, with the same hourly or sub-hourly resolution. Such data are scarcely available in most cases. Furthermore, it is not given that measurements from normal operation of buildings provide datasets that are 'rich' enough (containing enough statistical variability) to successfully drive the identification process. In (Sourbron, Verhelst, & Helsen, 2012), the authors conclude that the building control system should cause sufficient excitation of the building components whenever possible in test periods. This paper presents a method that aims at overcoming this bottleneck by combining features of both white-box and grey-box modelling. A set of white-box models (specifically, IDA-ICE models) representing the Norwegian stock of apartment blocks is available, based on ca. 20 archetypes previously developed in the TABULA/EPISCOPE project (Rønneseth & Sartori, 2018). Validation of the hourly load profiles of such archetypes against a large dataset of measurements is undergoing in a parallel research activity. Provided that load profiles are validated, it is legitimate to assume that the indoor temperature profiles from the IDA-ICE archetypes are also representative for the real building stock. Under this assumption, the grey-box models can be identified from simulation of the archetypes. A Pseudo Random Binary Sequence (PRBS), aiming at exploring a wide and rapidly changing set of indoor temperatures around the comfort zone, is applied as the control signal for the heating system. Finally, validation of the identified models will focus on short term predictions (one day to one week) as this is the typical range of control horizon for predictive controllers.

Methods

For the model identification process, datasets from IDA-ICE simulations, using archetype models of Norwegian apartment blocks is used. Datasets from twenty-one variations of eight archetypes have been made available through a parallel activity in ZEN.

Table 1. Overview of archetypes.

Name	Building year	# of floors/apartments	Floor area [m^2]
AB_01	< 1956	4 / 8	557
AB_02	1956-1970	4 / 16	1115
AB_03	1971-1980	4 / 24	1672
AB_04	1981-1990	4 / 24	1672
AB_05	1991-2000	4 / 24	1672
AB_06	2001-2010	4 / 24	1672
AB_07	2011-2020	4 / 24	1672
AB_08	>2020	4 / 24	1672

Each archetype is a representative apartment block from each decade, with the exception of "AB_01", which represents apartment blocks built before 1956, and "AB_08", representing the passive house standard. The building standard (most importantly, the insulation) improves as the buildings get newer. Table 1 summarizes the archetypes.

Figure 1 shows the standard layout of the archetypes as they are modelled in IDA-ICE. A common method used when modelling multi-story buildings is to use a three-story building, with multipliers for the middle zones. This reduces both modelling and simulation time, without sacrificing accuracy in the results. Each apartment consists of three zones: living room, bedroom and bathroom (Rønneseth & Sartori, 2018). However, because the controlled heating input in the living room and bedroom is waterborne (district heating), and the bathroom is equipped with electric floor heating, the bathroom is disregarded. To find a representative temperature for the apartment block, a weighted average of the temperatures is taken, with the temperatures on the middle floor weighted by 2, since we are dealing with 4 floors.

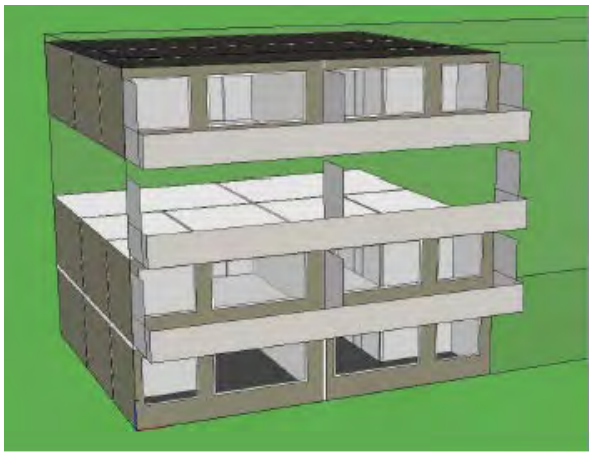

Figure 1. Apartment block layout in IDA-ICE (Rønneseth & Sartori, 2018).

The IDA-ICE simulations are done for a typical meteorological year (TMY) (Renné, 2016), with a Pseudo-random binary signal (PRBS) applied to the heating control system. The signal is applied from the 1st to the 20th in every month of the year. One issue with the signal is that it is applied to the zone-level heaters in the IDA-ICE models, while there still is a weather compensation curve modulating the supply temperature of the waterborne heating system. Thus, the signal is not a true PRBS, since the heating power has a certain dependancy on the outdoor temperature. Figure 2 shows the extracted dataset for "AB_03" in May. We see that the indoor temperature yTi is allowed to deviate substantially from normal comfort limits.

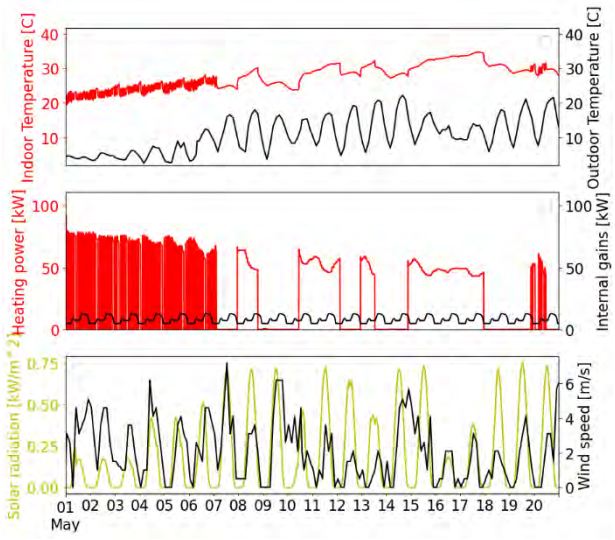

Figure 2. Example input dataset.

To identify suitable models from the data, the forward selection procedure in (Bacher & Madsen, 2011), which uses maximum likelihood estimation, is employed. Consider a series of measurements:

$$Y_n = [y_n, y_{n-1}, \cdots, y_1, y_0] \quad (1)$$

The likelihood function is the joint probability density:

$$L(\theta; Y_n) = p(Y_n|\theta) \quad (2)$$

where θ is the vector of model parameters. Another way to write this is:

$$L(\theta; Y_n) = \left(\prod_{k=1}^{N} p(Y_k|Y_{k-1}, \theta)\right) p(Y_0|\theta) \quad (3)$$

i.e. as a product of conditional densitities, with $p(Y_0|\theta)$ as a parameterization of the starting conditions (Kristensen, Madsen, & Jørgensen, 2004). The set of parameters $\hat{\theta}$ that maximizes the likelihood of the model is then found by solving to the optimization problem:

$$\hat{\theta} = arg\ \max_{\theta}\{L(\theta; Y_N)\} \quad (4)$$

The software CTSM-R, developed at DTU, is used to identify the models. CTSM-R, or Continuous Stochastic Time Modelling in R, is an R package providing a framework for identifying and estimating stochastic grey-box models. A grey-box model consists of a set of stochastic differential equations coupled with a set of discrete time observation equations, which describe the dynamics of a physical system and how it is observed. The grey-box models can include both system and measurement noise, and both nonlinear and nonstationary systems can be modelled using CTSM-R . Internally, it uses an extended Kalman filter to set up the conditional densities from the parametrized initial conditions, and a quasi-Newton method for solving the optmization problem (Madsen, 2018). An issue with gradient-based methods in general is that it finds a local optimum, i.e., there is no guarantee that the solution found is the most optimal on the entire parameter space.

A forward selection process is employed by utilizing a statistical test, in which each model considered is a subset of a larger model (Bacher & Madsen, 2011). The starting point for the procedure is the smallest feasible model, and possible improvements are added successively until the maximum amount of information is extracted from the data. The criteria for this is a statistical testing procedure involving likelihood-ratio tests: when the p-value is below a certain limit (e.g. 0.05, which corresponds to a 95 %-confidence level), the more complex model is selected in favor of the simpler model. If no additions yield a p-value below the limit, we have found a sufficient model. We start the selection procedure with the smallest feasible model:

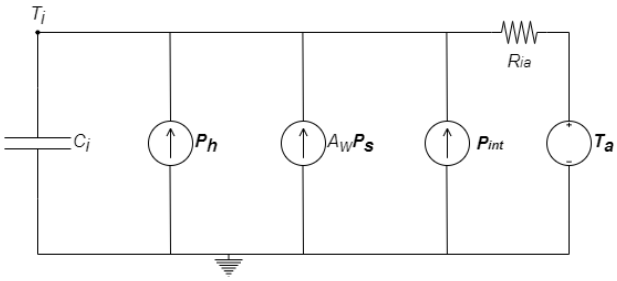

Figure 3. Model Ti

$$dT_i = \frac{1}{R_{ia}C_i}(T_a - T_i)dt + \frac{1}{C_i}(P_s + P_h + P_{int})dt + \sigma_i d\omega_i \quad (5)$$

$$Y_k = T_{i,k} + e_i \quad (6)$$

with descriptions of the variables and parameters listed below. Since we are dealing with mathematical models, it is most accurate to characterize the descriptions as *interpretations* in the case of parameters found with maximum likelihood estimation. The physical meaning for the same parameter will change as the model order increases (Bacher & Madsen, 2011):

T_i – Indoor air temperature

T_a – Outdoor temperature

C_i – Thermal capacitance of interior

R_{ia} – Thermal resistance from interior to ambient

A_w – Effective window area

σ_i – Variance of the Wiener (stochastic) process

Following the example of (Bacher & Madsen, 2011), states to add in the forward selection process are T_m and T_e. They represent the temperature of the heat transportation medium and building envelope respectively. For conciseness,

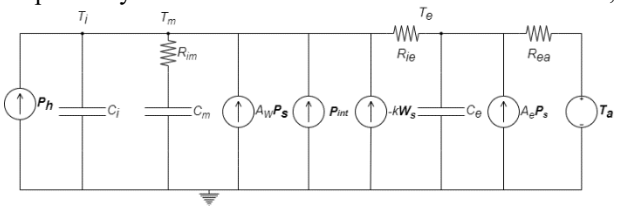

Figure 4. Model TiTeTmAeWs

only the equations and circuit diagram for the complete model *TiTeTmAeWs* are shown here. These two additional states result in two additional state equations. Furthermore, a renaming of the resistance associated with the interior from R_{ia} (directly from interior to ambient) to R_{ie} (from interior to envelope) is necessary, as well as substituting T_a with T_e in equation 5:

$$dT_i = \frac{1}{R_{ie}C_i}(T_e - T_i)dt + \frac{1}{R_{im}C_i}(T_m - T_i)dt + \frac{1}{C_i}(P_s + P_h + P_{int} - k * Ws)dt + \sigma_i d\omega_i \quad (7)$$

$$dT_m = \frac{1}{R_{im}C_m}(T_i - T_m) + \sigma_m d\omega_m \quad (8)$$

$$dT_e = \frac{1}{R_{ie}C_e}(T_i - T_e)dt + \frac{1}{R_{ea}C_e}(T_a - T_e)dt + \sigma_e d\omega_e \quad (9)$$

where the added parameters are:

T_e - Envelope temperature

T_m – Medium temperature

R_{ie} - Thermal resistance from interior to envelope

R_{ea} - Thermal resistance from envelope to ambient

R_{im} – Thermal resistance from interior to medium

C_m – Thermal capacitance of medium

C_e - Thermal capacitance for the envelope

σ_e – Wiener process variance for T_e

σ_m – Wiener process variance for T_m

k – Wind heat transmission coefficient [unit: $\frac{K*s}{kWh*m}$]

Generally, the grey-box models considered in this work can be expressed as continuous, stochastic state-space matrix equations. This can be written as:

$$d\mathbf{T} = \mathbf{A}\mathbf{T}dt + \mathbf{B}\mathbf{U}dt + \mathbf{E}\mathbf{V}dt + d\boldsymbol{\omega} \quad (10)$$

where **T** is the temperature state vector, **U** is the controllable input vector, and the transition matrices **A** and **B** consist of simple parameters only to preserve model linearity. This also applies to the matrix **E**, which contains the coefficients for the disturbance vector **V**, where uncontrolled heating inputs are lumped. The term $d\boldsymbol{\omega}$ represents the stochastic part of the model, which is represented by the Wiener process.

After model identification and p-value testing, models are validated using datasets from normal operation, i.e. the heating control system trying to maintain a constant set-point temperature (no nighttime setback). Figure 5 shows the entire model identification process, from IDA-ICE simulation to validation of the models. Processes are colored green, data is colored light blue, and decisions purple. Notice the stippled lines around the IDA-ICE simulation with PRBS-signals, which is an ongoing parallel research activity.

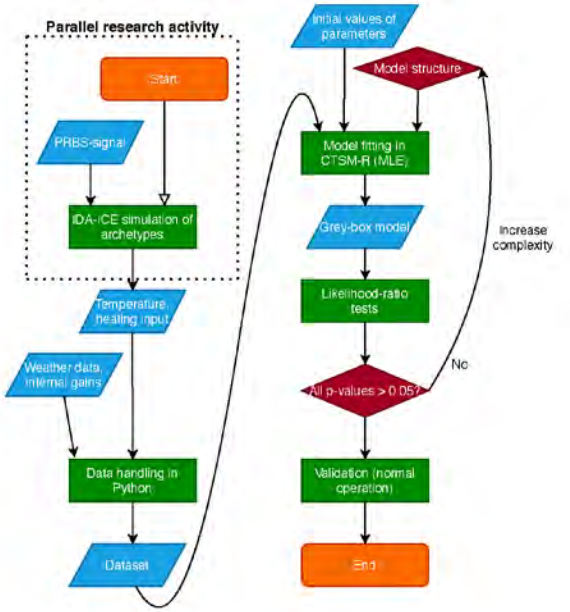

Figure 5. Flowchart of the model identification process.

Results

Due to the large number of archetypes and models that have been investigated in the work leading up to this paper, the presentation of results will be limited to the archetype "AB_03" variant 2 for space considerations (apartment block from the seventies, windows changed, renovated). We consider this to be a good representation of the "average" apartment block in the Norwegian building stock. Furthermore, of all the models identified, the ones from the training dataset in May are presented, since this month has the most variability with regard to solar radiation and outdoor temperature. For validation, the models identified in CTSM-R, which are continuous time state-space models, are discretized in accordance with the time step of the of the dataset used for training (5 min). First, we consider the results from the p-value test.

Table 2. Forward selection, AB_03 var 2, May

Iteration		**Models**		
0	*Ti*			
# params	6			
$l(\theta; Y_n)$	389.22			
1	*TiTe*	*TiTm*	*TiAe*	*TiWs*
# params	10	10	n.a.	7
$l(\theta; Y_n)$	1769.12	1773.16	n.a.	389.22
p-value	0	0	n.a.	0.29
2	*TiTeTm*	*TiTeWs*	*TiTeAe*	
# params	14	11	11	
$l(\theta; Y_n)$	1828.35	1765.28	1470.86	
p-value	0	1	1	
3	*TiTeTmWs*	*TiTeTmAe*		
# params	15	15		
$l(\theta; Y_n)$	1828.35	1829.27 (?)		
p-value	1	0.17		
4	*TiTeTmAeWs*			
# params	16			
$l(\theta; Y_n)$	1829.27			
p-value	1			

For the May dataset, the p-value test suggests both *TiTe* and *TiTm* as improvements on the one-state model *Ti*, with a p-value of 0 for both. This signifies that the models describe the data significantly better than the one-state model. Since *TiTm* has a slightly higher log-likelihood, this is the model selected in the first iteration. The model with wind speed (**Ws**) added as a disturbance generator does not yield any improvement on the log-likelihood, hence this model is dropped and the extension saved for later. In the next iteration, the only model that yields any improvement is the three-state model *TiTeTm*. The other extensions actually yield lower log-likelihoods than the best models in the previous iteration.

In the third iteration, the extensions **Ae** (splitting of solar gains in internal and envelope parts) and **Ws** do not yield any significant improvements over *TiTeTm*. Strictly speaking, the model selection process should end here, but for completeness, we try fitting the full model. It has the same log-likelihood as *TiTeTmAe*, thus, there is no improvement. Hence, the model selection process is finished, with *TiTeTm* as the "winner".

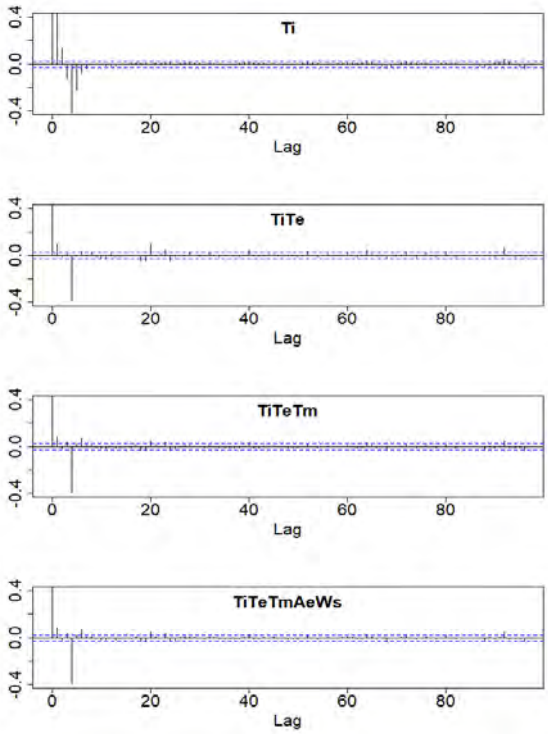

Figure 6. ACF of the residuals

To investigate the assumption of white-noise residuals (effects not captured by the model are uncorrelated and identically and independently distributed), we look at the autocorrelation function of the residuals. It shows the correlation of the residuals ($Y - \hat{Y}$) in the time domain. For this assumption to hold with a 95 % confidence level, ca. 19 of 20 lags have to be inside the blue line in the plots.

Figure 6 shows the autocorrelation of the residuals for a selection of the models considered in the forward selection process. For the one-state model, *Ti*, visual inspection of the ACF-plot tells us that at least 7 out of the

96 lags shown in the plot is outside the 95 % confidence interval, thus, the model does not describe the heat dynamics of the apartment block sufficiently. For the two-state-model, *TiTe,* the lags from timestep zero to seven are dampened, but there is an emergence of lags around timestep 20 that was not present in the previous model. Counting the lags yields 5 terms outside the confidence interval. Hence, this model is also insufficient for describing the heat dynamics. The next model, *TiTeTm,* shows a dampening of the lags around timestep 20, and they appear now to be within the confidence band, and we have three lags outside it. This means that the white-noise assumption on the residuals holds. The complete model, *TiTeTmAeWs,* shows no improvement, and it can be concluded that judging by the autocorrelation plots, the model *TiTeTm* is a sufficient model.

To test the prediction performance of the models identified, we look at the open-loop out-of-sample predictions for a selection of the models (*TiTe, TiTe, TiTeTm*). The validation datasets contain data for normal operation of the heating system, i.e. keeping the zones at a constant 20 degrees Celsius (there is no nighttime lowering of the temperature). In order to get a reasonable estimate of the hidden states (in our case, T_m and T_e), a one-step ahead prediction, where the correct ("measured") temperature is fed back to the model, is run for 48 hours immediately preceding the week selected for open-loop prediction. This should give a better estimate of the hidden states than the naïve approach of simply setting them equal to the value of T_i at the start of the validation period.

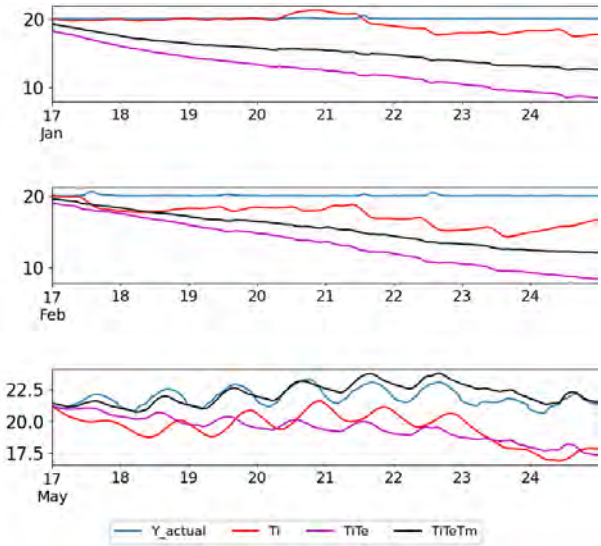

Figure 7. Validation, May models (Jan., Feb., May)

Figure 7 shows the prediction open-loop prediction of the models *Ti, TiTe*, *TiTeTm* and *TiTeTmAeWs* identified with PRBS-operation in May on validation datasets with normal operation in January, February and May. From the plots, it can be seen that the models generally fails in the winter months of January and February. An exception here is the one-state model *Ti*, which manages to track the actual temperature for almost 4 days. This may be due to the total capacitance being smaller than for the other models (see table 2.), i.e. needing less heat to maintain the set-point temperature. In addition, the effective window area estimated for *Ti* is on the smaller side, at 11.25 m^2, which makes gives the solar gains relatively little importance in the model, making it more consistent with the moderate solar radiation in January. We see the same trend in February, *Ti* tracks the set-point temperature best, but here there is drop-off after 12 hours, and although the model recovers somewhat, there is a persistent offset of at least 1 degree Celsius. For validation in May, the predictions from *TiTeTm* follows the actual temperature for 4 days, which has to be considered good prediction performance in this context.

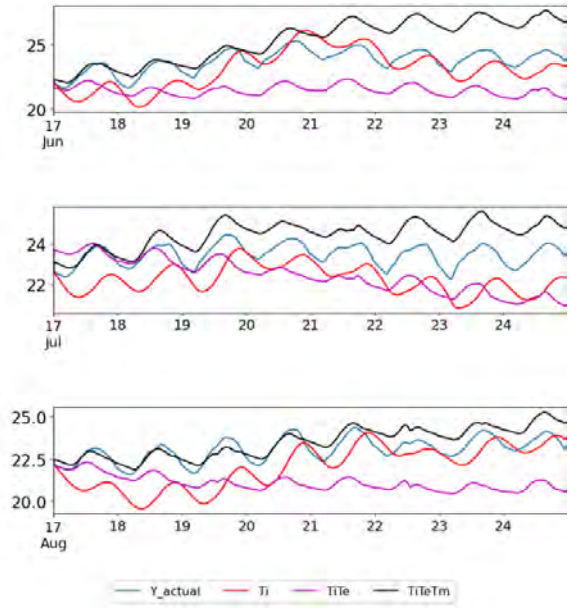

Figure 8. Validation, May models (June, July, Aug.)

Figure 8 shows the open-loop predictions of models identified in May on validation datasets in June, July and August. It can immediately be seen that prediction performance is better in these months than in the winter months. The model *TiTeTm* again appears to have to best performance, although there is an issue with the initial conditions. The temperature (of the interior, "measured") jumps up immediately after the first time step, which signifies that the estimation of the initial values of the hidden states is too high. We can interpret this as one or more of the hidden states having a biased energy balance. Indeed, by looking at table 3, it is seen that the estimated initial value of the medium temperature, T_{m0}, is estimated to -24.6 °C for both the complete model and *TiTeTm*. This is clearly a non-physical situation; the heat transportation medium should not have a temperature that is higher than the envelope. According to (Coninck, Magnusson, Åkesson, & Helsen, 2016), this is a situation in which numerical optimality should be balanced against models with parameters that make sense physically. A less optimal in the numerical sense, i.e. a model with a lower log-likelihood, can be a more beneficial model for prediction and forecasting, given that it has sensible

parameters, not necessarily in the absolute numbers, but at least in relative terms. This non-physicality can also be inferred from the estimated time constants and UA-values[W/°Cm^2]: the time constant of the envelope ranges from 137 to 218 hours as different topologies are considered, and the UA-values range from 0.83 to 7.88. Searching the entire parameter space for both numerically feasible and physically sensible models with a gradient-based method is not a trivial task, and no attempt to solve this in a systematic fashion has been undertaken in this work.

Table 3. Model parameters, identification May

Parameters	***TiTeTmAeWs***	***TiTeTm***	***TiTe***	***Ti***
T_{i0} [°C]	19.39	19.39	19.37	25.47
T_{e0} [°C]	20.08	20.14	19.30	n.a.
T_{m0} [°C]	-24.60	-24.59	n.a.	n.a.
C_i kWh/°C]	8.20	8.27	5.04	75.16
C_e [kWh/°C]	1024	488.3	2939	n.a.
C_m [kWh/°C]	0.30	0.33	n.a.	n.a.
R_{ie} [°C/kW]	0.013	0.013	0.015	*0.49
R_{im}[°C/kW]	0.58	0.55	n.a.	n.a.
R_{ea}[°C/kW]	0.18	0.28	0.075	n.a.
A_w[m^2]	89.39	102.52	81.76	11.25
A_e [m^2]	178.0	n.a.	n.a.	n.a.
e_i	-5.60	-5.61	-16.3	-25.5
σ_i	-8.35	-8.35	-0.63	-0.90
σ_m	3.71	3.66	n.a.	n.a.
σ_e	-0.98	-1.01	-0.72	n.a.
τ_1 [h]	0.102	0.102	0.074	36.99
τ_2[h]	0.184	0.192	n.a.	n.a.
τ_3 [h]	181.06	137.66	218.4	n.a.
C_{tot} [kWh/°C]	1033	496.9	2944	75.16
UA [W/°Cm^2]	0.905	0.835	7.88	1.42

We consider instead models identified in September, which yielded more consistent results. Figure 9 shows the open-loop predictions on the same validation datasets as Figure 8. The prediction performance of *TiTe* especially is improved. Furthermore, the performance of the three-state model *TiTeTm* is also improved, with a closer tracking of the actual temperature in the timeframes where the May models showed satisfactory performance , and a decreased tencency to diverge towards the end of the weeks.

Table 4 shows the time constants and UA-values for a selection of the models identified on the September dataset. The consistency across the model topologies is a significant improvement on the models identified on the May dataset. . The UA-value lies between 1.51 and 1.64, values that can be considered reasonable. The smallest

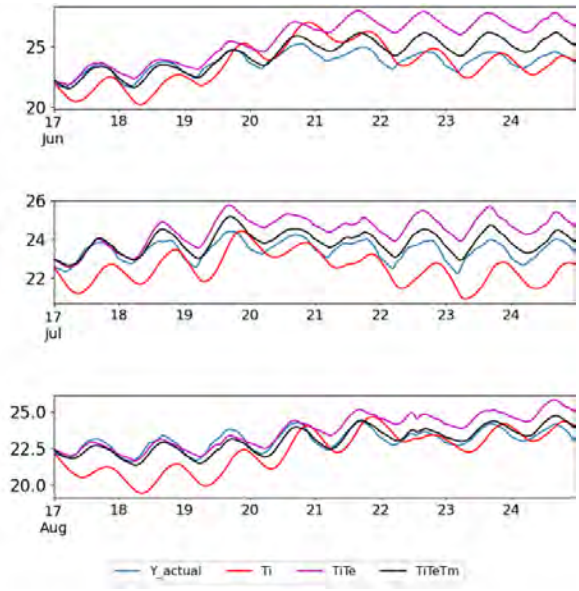

Figure 9. Validation, Sept. models (June, July, Aug.)

time constant is right around the sampling time of 0.0833 hours in the topologies with more than one state. This makes sense, as this is the smallest timeframe in which any dynamics can be captured by the model. If a sampling time of one hour were to be used instead, a small time constant of around 1 hour would be seen instead.

Table 4. Essential model parameters, identification September

Parameters	***TiTeTmAeWs***	***TiTeTm***	***TiTe***	***Ti***
τ_1 [h]	0.073	0.061	0.101	32.84
τ_2 [h]	3.31	2.61	n.a.	n.a.
τ_3 [h]	131.32	125.5	90.78	n.a.
UA [W/°Cm^2]	1.51	1.52	1.64	1.53

Comparing identification results across archetypes is another indicator of the consistency of the results. Due to issues with opitmizer convergence and time limits, this exercise has been limited to the archetypes AB01.5 (old building, renovated windows), AB03, AB07 and AB08 in this work. Table 5 shows the results. There is a difference in how the resistances and capacitances are handled, e.g. for AB_01, the resistances are higher than for AB_07 (which corresponds to TEK10) and AB_08 (passive house standard). On the other hand, if the capacitances are taken into account, the results make more sense. As the building standard increases, the time constants increase. This is in line with the expected: because of better insulation in the walls, there is a larger tendency for the heat to remain in the envelope. As for the UA-value, it decreases in accordance with the building standard, with the exception of AB_03, where it increases.

Table 5. Model parameters across archetypes, TiTe, May dataset

Parameters	***AB01.5***	***AB03***	***AB07***	***AB08***
T_{i0}[°C]	19.24	19.37	21.16	21.79
T_{e0}[°C]	19.12	19.30	21.11	21.76
C_i [kWh/°C]	1.70	5.04	20.15	26.04
C_e [kWh/°C]	310.8	2939	755.0	892.7
R_{ie} [°C/kW]	0.036	0.015	0.005	0.0045
R_{ea}[°C/kW]	0.39	0.074	0.30	0.39
A_w[m^2]	176.62	81.76	164.8	162.4
e_i	-17.51	-16.28	-8.73	-9.13
σ_i	-0.83	-0.63	-9.83	-10.10
σ_e	-1.04	-0.72	-1.69	-1.74
τ_1 [h]	0.608	0.074	0.104	0.113
τ_2 [h]	122.1	218.4	233.0	355.0
UA [W/°Cm^2]	4.93	7.88	2.33	1.79

To compare the parameters obtained through model identification in CTSM-R with the parameters of the IDA-ICE models, some assumptions are necessary. Although reports of the simulation models are available, they do not contain any information about the thermal capacity of the apartment blocks. To alleviate this, we use (Standard Norge, 2014) to get approximate values for the capacitances. Assuming a relatively heavy building (100 Wh/Km^2), and a ceiling height of 2.7 m, the envelope thermal capacity can be calculated. The thermal capacity of the interior is more straightforward, taking 0.342 Wh/m^{3}K as the specific heat capacity of air at 15 °C (Dixon, 2007; Jones, 1978). The per floor area normalized heat transfer coefficient UA is found from simulation reports in IDA-ICE. If it is assumed that the most of the thermal resistance is connected to the envelope, an approximation of the long time constant can be found by multiplying the envelope capacitance and the total thermal resistance (inverse of the UA-value), since these are the parameters that dominates the dynamics of the system at low frequencies. Table 6 shows the results of this estimation. As can be seen from the table, both the capacitances and the UA-values are overestimated by a significant margin. However, the time constants are quite close, which means that the overestimation of the capacitances and the underestimation of the resistances balance each other out to yield a seemingly good estimate of the time constants, and hence the heat dynamics of the buildings. Nevertheless, it must be kept in mind that the values we are comparing the estimated model parameters to are estimates themselves, so further investigation into the possibility for a more thourough reporting of the IDA-ICE model is needed.

Table 6. Estimated/reported parameters (IDA-ICE)

Parameters	***AB01.5***	***AB03***	***AB07***	***AB08***
C_i [kWh/°C]	0.5	1.5	1.5	1.5
C_e [kWh/°C]	60	160	160	160
UA [W/°Cm^2]	0.98	0.51	0.39	0.25
τ_2 [h] (apprx.)	120	188	246	380

Discussion

The results from the model identification are varied. For some validation datasets, the open-loop prediction performance may be regarded as sufficiently adequate for MPC application purposes (with prediction horizon typically from one to few days, and actuation of only 1-step ahead control signal in closed loop). This is generally in the months with little to no controllable heat input (summer months). In the winter months, however, only the single-state model *Ti* is able to track the actual temperature. An explanation could be that the indoor temperature – from the IDA ICE archetypes – in these months is almost constant, which is an unrealistic situation in real life. Were there more variability in the measured temperature, the model could perhaps capture these dynamics. This aspect might be improved by changing the low-level controllers of the heating system in the IDA-ICE archetypes, which are now simulated as an ideal PI-controller.

Furthermore, as was mentioned in the Methods section, there is also some modulation of the heating input through a weather compenstion curve in the central heating system in the IDA-ICE model, which means that the heating signal is not pure PRBS. Hence, the heating input in May is significantly smaller than in January. However, in January, the solar radiation is small, so this would mean that the models will have poor prediction performance on the months with more significant solar radiation. May should be a good a compromise with regard to the trade-off between heating and solar. In the results, better prediction and more consistent parameter estimates were shown for September, but the same argument could be made for this month. There is also the possibility of bugs in the IDA-ICE archetype models beyond this. However, since IDA-ICE simulation is not the topic of this paper, this is left for further work.

Another point of uncertainty is the merging and weighing of the temperatures for the different zones. It could be that this simple approach smoothes out dynamics in the temperature that might be needed for better and more consistent results from the model identification. To investigate this further, a model with zoning could be set up. These models, however, would quickly become convoluted, with many parameters and states, and would increase the computational time needed for convergence of the log-likelihood optimization by an order of magnitude.

Nevertheless, it could simply be that there is not enough variability in datasets generated from simulation software to drive the model identification process. This aspect is worth further investigation, especially with respect to the low-level controls (i.e. PI controller) in the simulated heating system, since this maintains an unrealistically constant (and challenging from a statistical analysis viewpoint) indoor temperature.

Conclusion

The software package CTSM-R has been used in order to obtain reduced-order models, based on data from the building simulation program IDA-ICE, obtained by using a Pseudo-random binary signal. A forward selection procedure is employed to find a model that sufficiently describes the data. A three-state model, *TiTeTm*, is found to the best alternative, both in the log-likelihood p-value test, and in the validation performance. In the weeks selected for validation, the models identified on the Septemeber dataset shows better prediction performance than the models identified on the May dataset. These parameters of these models also exhibit more reasonable physical values. In general, the models perform better on the validation datasets when there is no controlled heating input.

Acknowledgement

This paper has been written within the Research Centre on Zero Emission Neighbourhoods in Smart Cities (FME ZEN), grant nr. 257660, and within the research project Low Temperature Thermal Grids (LTTG), grant nr. 280994. The authors gratefully acknowledge the support from both the ZEN and LTTG partners and the Research Council of Norway

References

Bacher, P., & Madsen, H. (2011). Identifying suitable models for the heat dynamics of buildings. *Energy and Buildings*, *43*, 1511–1522. https://doi.org/10.1016/j.enbuild.2011.02.005

Coninck, R. De, Magnusson, F., Åkesson, J., & Helsen, L. (2016). Toolbox for development and validation of grey-box building models for forecasting and control. *Journal of Building Performance Simulation*, *9*(3), 288–303. https://doi.org/10.1080/19401493.2015.1046933

Dixon, J. C. (2007). Appendix B: Properties of Air. In *The Shock Absorber Handbook* (pp. 375–378). https://doi.org/10.1002/9780470516430.app2

Jones, F. E. (1978). The Air Density Equation and the Transfer of the Mass Unit. In *Journal of Research of the National Bureau of Standards* (Vol. 83).

Kristensen, N., Madsen, H., & Jørgensen, S. (2004). Parameter Estimation in Stochastic Grey-Box Models. *Automatica*, *40*, 225–237. https://doi.org/10.1016/j.automatica.2003.10.001

Madsen, H. et. al. (2018). *Continuous Time Stochastic Modeling in R User's Guide and Reference Manual*. Retrieved from http://ctsm.info/pdfs/ctsmr-reference.pdf

Renné, D. S. (2016). Resource assessment and site selection for solar heating and cooling systems. In R. Z. Wang & T. S. Ge (Eds.), *Advances in Solar Heating and Cooling* (pp. 13–41). https://doi.org/https://doi.org/10.1016/B978-0-08-100301-5.00002-3

Rønneseth, Ø., & Sartori, I. (2018). *Possibilities for Supplying Norwegian Apartment Blocks With 4 Th Generation District Heating*.

Sourbron, M., Verhelst, C., & Helsen, L. (2012). Building models for model predictive control of office buildings with concrete core activation. *Journal of Building Performance Simulation*, *6*, 1–24. https://doi.org/10.1080/19401493.2012.680497

Standard Norge. (2014). *Calculation of energy performance of buildings - Method and data*. Retrieved from https://www.standard.no/no/Nettbutikk/produktkatalogen/Produktpresentasjon/?ProductID=702386

Walnum, H. T., Sartori, I., & Lindberg, K. B. (2019). Influence of inputs knowledge on Grey-box models for Demand Response in Buildings. *Proceedings of Building Simulation 2019: 16th Conference of IBPSA*.

Xingji Y., Laurent, G. I., & Sartori, I. (2019). Investigation of the Model Structure for Low-Order Grey-Box Modeling of Residential Buildings. *IBPSA Nordic BuildSim Nordic Conference 2019*.